

Supplementary Information

Large-Area, lithography-free, narrow-band and highly-directional thermal emitter

Xingxing Liu, Zhiwei Li, Zhengji Wen, Mingfei Wu, Jialiang Lu, Xu Chen, Xinchao Zhao, Tao Wang, Ruonan Ji, Yafeng Zhang, Liaoxin Sun, Bo Zhang, Hao Xu, Jing Zhou, Jiaming Hao*, Shaowei Wang*, Xiaoshuang Chen, Ning Dai, Wei Lu and Xuechu Shen

Note 1: The temperature-dependent absorption/emission properties of the thermal emitter

To investigate the temperature-dependent absorption /emission properties of the thermal emitter, the optical properties of materials at different temperatures should be considered. For zinc sulfide (ZnS) and germanium (Ge), the temperature-dependent dielectric function can be described by the following expressions^[S1-S3] in the range of our interest (wavenumbers from 900 cm⁻¹ to 1000 cm⁻¹, and temperatures from 300 K to 400 K):

$$\varepsilon_{ZnS} = (A_1 + B_1\lambda + C_1\lambda^2 + D_1\lambda^3 + E_1\lambda^4)^2 \quad (S1)$$

where $A_1 = 1.973 \times 10^{-4}T + 2.304$, $B_1 = -8.671 \times 10^{-6}T - 1.563 \times 10^{-2}$, $C_1 = 5.549 \times 10^{-7}T + 2.067 \times 10^{-3}$,
 $D_1 = 2.597 \times 10^{-8}T - 1.714 \times 10^{-4}$, $E_1 = -9.798 \times 10^{-10}T + 2.884 \times 10^{-6}$.

and
$$\varepsilon_{Ge} = A_2 + B_2\lambda^2 / (\lambda^2 - C_2) + D_2\lambda^2 / (\lambda^2 - E_2) \quad (S2)$$

where $A_2 = -6.040 \times 10^{-3}T + 12.30861$, $B_2 = 9.295 \times 10^{-3}T + 4.00536$, $C_2 = -5.392 \times 10^{-4}T + 0.599034$,
 $D_2 = 4.151 \times 10^{-4}T + 0.09145$, $E_2 = 1.51408T + 3426.5$.

On the other hand, the temperature dependent permittivity of gold is given by a modified Drude model^[S4-S6]:

$$\varepsilon_m(T) = \varepsilon_\infty - \frac{\omega_p^2(T)}{\omega^2 + i\omega\gamma(T)} \quad (S3)$$

where ω is the angular frequency of the incident light, ε_∞ is the high-frequency permittivity of the metal. $\omega_p(T)$ denotes the plasma frequency and $\omega_p(T) = 1.37 \times 10^{16} \text{ rad/s}$, which is assumed as a constant over the range of temperatures. $\gamma(T)$ is the temperature-dependent electron collision frequency, where $\gamma(T) = \gamma(T = 308K) \times \left(\frac{T}{308}\right)^{1.3}$ with $\gamma(T = 308K) = 1.0027 \times 10^{14} \text{ rad/s}$. Based on the above models, we investigated the

temperature-dependent absorption properties of the thermal emitter and plotted the results in Figure S2 of this supplementary.

Note 2: Analytical relationships between Q factors and the geometrical parameters

According to the CMT^[S7-S9], we know the key point to maximize the absorbance/emittance at the resonant frequency is to match the absorptive quality factor Q_a with the radiative quality factor Q_r . Here we derive the relationships between these two Q factors with the geometrical parameters.

In principle, the scattering properties of the thermal emitter can be rigorously analyzed based on transfer matrix method^[S10]. For normal incidence, the electric field component E_y of the m -th layer can be written as

$$E_y^m = a_m e^{ik_z^m z} + b_m e^{-ik_z^m z}, \quad (\text{S4})$$

where a_m and b_m are the m -th layer forward and backward wave components, respectively. $k_z^m = (\omega/c)n_m$ is the m -th layer z -direction wave vector. Time variation term $e^{-i\omega t}$ is omitted for convenience.

According to Maxwell's equations, we can obtain the magnetic field component H_x of m -th layer

$$H_x^m = \frac{k_z^m}{\omega\mu_m\mu_0} \left(a_m e^{ik_z^m z} - b_m e^{-ik_z^m z} \right), \quad (\text{S5})$$

Suppose the dielectric constant ε_m of m -th layer is dispersive (no magnetic dispersion) and

can be modeled by a Lorentzian function $\varepsilon_m = \varepsilon_\infty \left(1 - \frac{\omega_p^2}{\omega^2 - \omega_0^2 + i\omega\Gamma_e^m} \right)$, then the time

average of the average energy density of the m -th layer is given by^[S11]

$$\bar{W}_m = \frac{\varepsilon_0}{4} \left(\varepsilon'_m + \frac{2\omega\varepsilon''_m}{\Gamma_e^m} \right) |E_m|^2 + \frac{\mu_0}{4} \mu_m |H_m|^2. \quad (\text{S6})$$

Therefore, the time-averaged energy $\langle U_m \rangle$ stored in m -th layer can be obtained by integration of the average energy density of the m -th layer

$$\langle U_m \rangle = \frac{\varepsilon_0}{4} \left(\varepsilon'_m + \frac{2\omega\varepsilon''_m}{\Gamma_e} \right) (A_m + B_m) + \frac{|k_z^m|^2}{4\mu_0\mu_m\omega^2} (A_m - B_m). \quad (\text{S7})$$

Where A_m and B_m are defined as:

$$\begin{cases} A_m = \frac{|a_m|^2}{i[k_z^m - (k_z^m)^*]} \left(e^{i[k_z^m - (k_z^m)^*]d_m} - 1 \right) + \frac{|b_m|^2}{-i[k_z^m - (k_z^m)^*]} \left(e^{-i[k_z^m - (k_z^m)^*]d_m} - 1 \right) \\ B_m = \frac{a_m b_m^*}{i[k_z^m + (k_z^m)^*]} \left(e^{i[k_z^m + (k_z^m)^*]d_m} - 1 \right) + \frac{a_m^* b_m}{-i[k_z^m + (k_z^m)^*]} \left(e^{-i[k_z^m + (k_z^m)^*]d_m} - 1 \right) \end{cases}, \quad (\text{S8})$$

Where d_m is the thickness of m -th layer.

The absorption power of the m -th layer $\langle P_a^m \rangle$ can also be derived as

$$\langle P_a^m \rangle = \frac{1}{2} \varepsilon_0 \varepsilon''_m \omega \int_0^{d_m} |E_m|^2 dz = \frac{1}{2} \varepsilon_0 \varepsilon''_m \omega (A_m + B_m). \quad (\text{S9})$$

If the material of m -th layer is non-dispersive, i.e., both the dielectric constant and the relative permeability are real and frequency-independent, the time averaged EM energy density can be reduced to

$$\bar{W}_m = \frac{\varepsilon_0}{4} \varepsilon_m |E_m|^2 + \frac{\mu_0}{4} \mu_m |H_m|^2, \quad (\text{S10})$$

And the two parameters A_m and B_m can be simplified as

$$\begin{cases} A_m = |a_m|^2 d_m + |b_m|^2 d_m \\ B_m = a_m b_m^* \frac{1}{2ik_z^m} \left(e^{2ik_z^m d_m} - 1 \right) + a_m^* b_m \frac{1}{-2ik_z^m} \left(e^{-2ik_z^m d_m} - 1 \right) \end{cases}, \quad (\text{S11})$$

Then, the m -th layer time-averaged stored energy $\langle U_m \rangle$ is given by

$$\langle U_m \rangle = \frac{1}{2} \varepsilon_0 \varepsilon_m \left(|a_m|^2 + |b_m|^2 \right) d_m \quad (\text{S12})$$

As the material of m -th layer is lossless, the absorption power within this layer equals zero $\langle P_a^m \rangle = 0$.

The total time-averaged stored energy and absorption power inside the structure can thus be obtained by $\langle U \rangle = \sum_{i=1}^n \langle U_i \rangle$ and $\langle P_a \rangle = \sum_{i=1}^n \langle P_a^i \rangle$, respectively.

Now we study the total radiation power $\langle P_r \rangle$, for the present structure shined by a normal incident wave with unit amplitude, we note that the reflected wave not only contains the wave radiated from the structure, but also that directly reflected by the non-resonant background. Thus, $\langle P_r \rangle$ can be evaluated as

$$\langle P_r \rangle = \int dS \cdot \frac{1}{2} \text{Re} \left[\left(\mathbf{E}_y^0 \right)^* \times \mathbf{H}_x^0 \right], \quad (\text{S13})$$

Finally, the absorptive (Q_a) and radiative (Q_r) quality factors can be obtained

$$Q_a = \frac{\omega_0 \langle U \rangle}{\langle P_a \rangle} \Big|_{\omega = \omega_0}; \quad Q_r = \frac{\omega_0 \langle U \rangle}{\langle P_r \rangle} \Big|_{\omega = \omega_0} \quad (\text{S14})$$

Note 3: Retrieving Q factors based on experimental and numerical simulation results

For comparison, we can retrieve Q_a and Q_r from the experimental and numerical results, according to CMT (see Eq. (1) in the main text), the reflectance at resonance for our structure should be

$$R = \left(\frac{Q_r - Q_a}{Q_r + Q_a} \right)^2 \quad (\text{S15})$$

Meanwhile, the total Q factor of the structure is

$$Q = \frac{f_0}{\Delta f} = \frac{Q_a \cdot Q_r}{Q_a + Q_r} \quad (\text{S16})$$

where f_0 is the resonance frequency, Δf is full width at half maximum (FWHM) i.e. the bandwidth over which the power of vibration is greater than half the power at the resonant frequency.

We can easily identify the three parameters (f_0, R, Q) from the measured/simulated reflection spectra. From Equations (S15)-(S16), we finally obtain the two important parameters Q_a and Q_r from the retrieved R and Q , as shown in Equation (S17).

$$\left\{ \begin{array}{l} Q_a = \frac{2Q}{1-\sqrt{R}} \\ Q_r = \frac{2Q}{1+\sqrt{R}} \end{array} \right. \text{(Underdamped)} \quad \text{or} \quad \left\{ \begin{array}{l} Q_a = \frac{2Q}{1+\sqrt{R}} \\ Q_r = \frac{2Q}{1-\sqrt{R}} \end{array} \right. \text{(Overdamped)} \quad (\text{S17})$$

The obtained Q factors retrieved by numerical simulation results are plotted in Fig.S3, which show excellent agreements with Fig.4 in the main text demonstrated the validity of our proposed model.

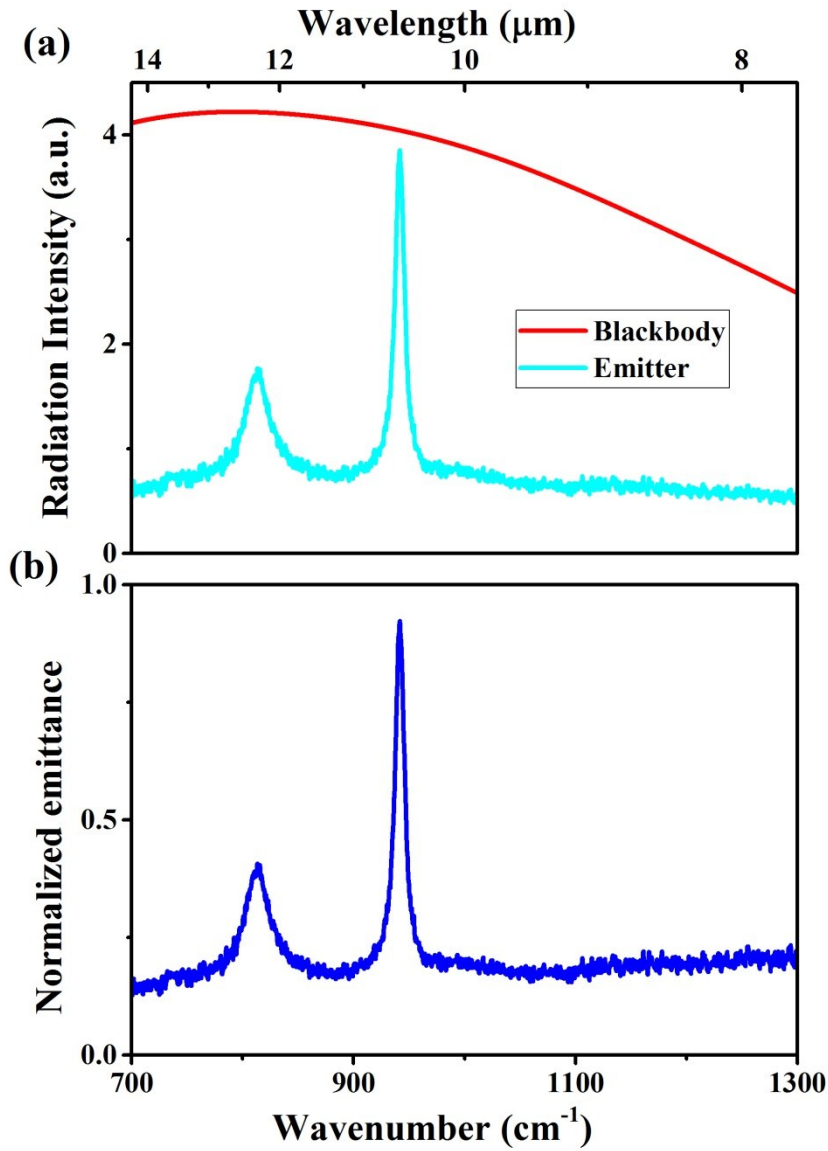


Figure S1 Thermal emission characteristics of fabricated thermal emitter and a blackbody control sample. (a) thermal emission spectra of fabricated thermal emitter and a blackbody control sample carbon nanotube array in the surface normal direction. **(b)** Normalized emittance of fabricated thermal emitter. The normalized emittance has a peak value of 92% at the wavenumber of 943.4cm^{-1} .

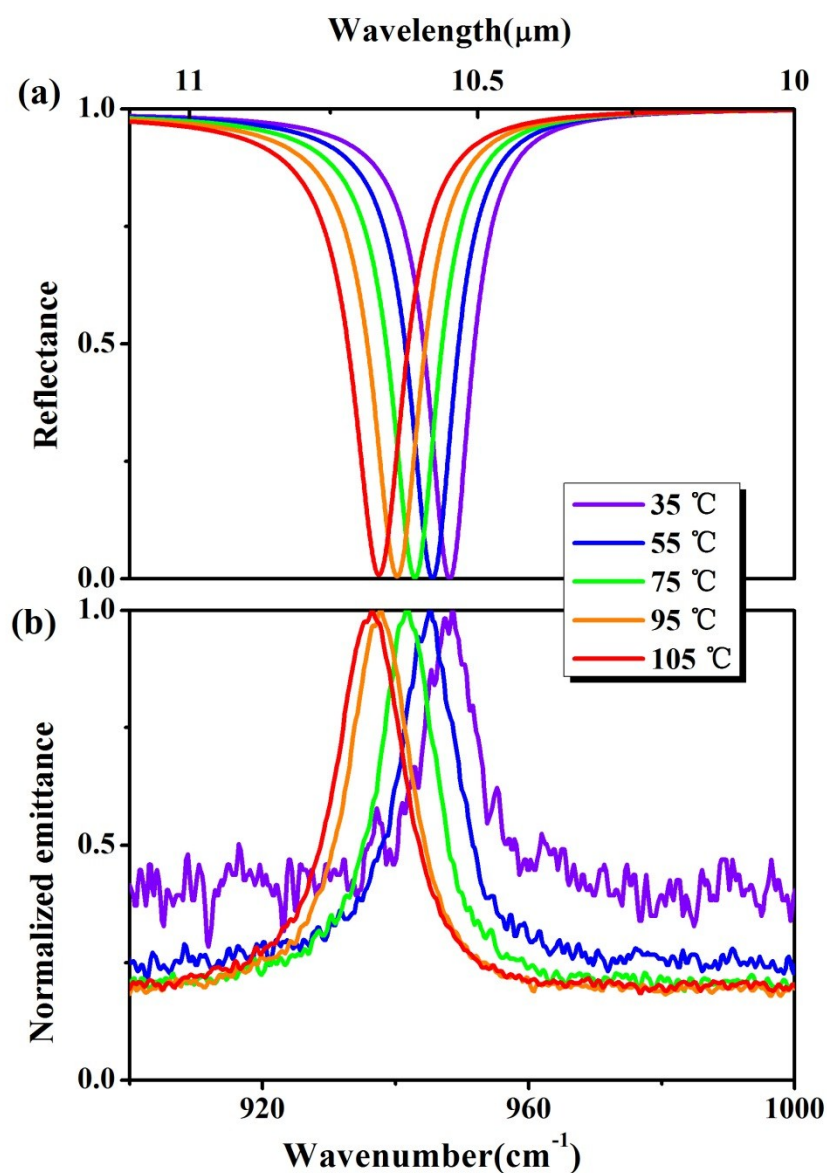


Figure S2 Temperature-dependent reflection and emission spectra of the thermal emitter. (a) calculated reflectance spectra of the thermal emitter for different temperatures. (b) the normalized experimental emittance spectra of fabricated thermal emitter for different temperatures. With the temperature increasing, the experimental thermal emission peaks show redshift, which is verified by the theoretical results.

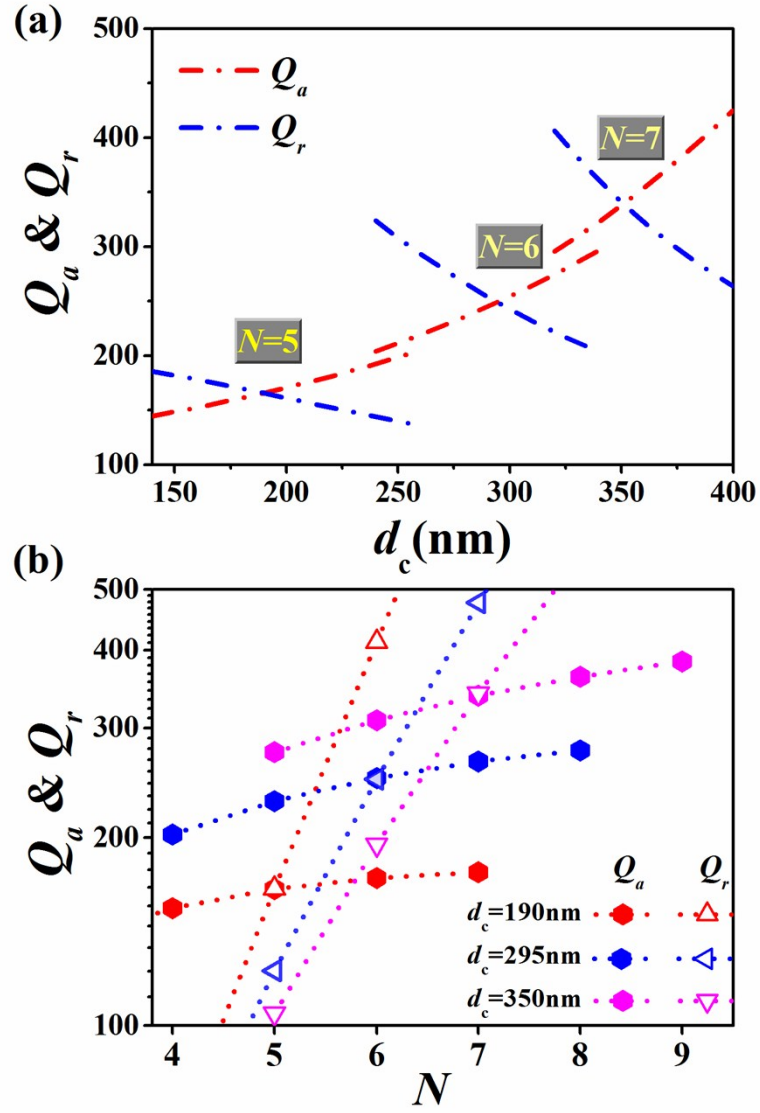


Figure S3 Retrieved Q factors from the numerical simulation results. (a) retrieved Q_a and Q_r as functions of the thickness of dielectric spacer d for the thermal emitters with three different number of photonic crystal periods. **(b)** retrieved Q_a and Q_r as functions of the number of photonic crystal periods N for the thermal emitters with three different thicknesses of dielectric spacer.

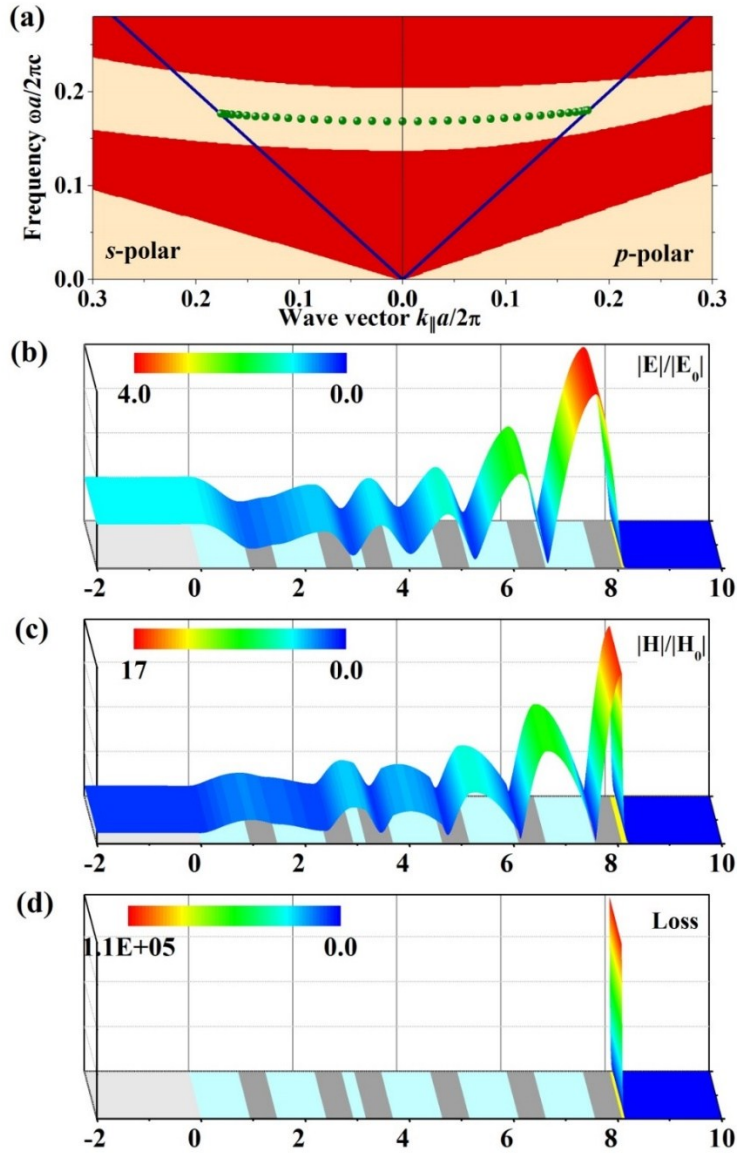


Figure S4 Projected band structure and electromagnetic field distributions. (a) Projected band structure of 1D photonic crystal with the light line (solid line) and resonant cavity modes located at the centre of photonic bandgap (solid symbols). In this design, the cavity layer is located at the third period of 1D photonic crystal and has a thickness of 240 nm. (b)-(c) the normalized electric and magnetic field amplitudes, respectively. (d) the time averaged power dissipation density for the same case in (b), (c).



Figure S5 Thermal emission image of a designed pattern based on the thermal emitter.

The thermal emission image was generated based on our thermal emitter, where the emitter was coated by a copper mask with a hollow pattern of the abbreviation of Shanghai Institute of Technical Physics (SITP) and was heated to 50 °C by a heating ceramic plate underneath. The image was recorded by an infrared camera with response wavelengths ranging 8~13 μm . This is in sharp contrast to the thermal images printed based on plasmonic nanostructures^[S12, S13], in which those patterns were usually encoded by using a huge number of the building blocks of plasmonic nanostructures.

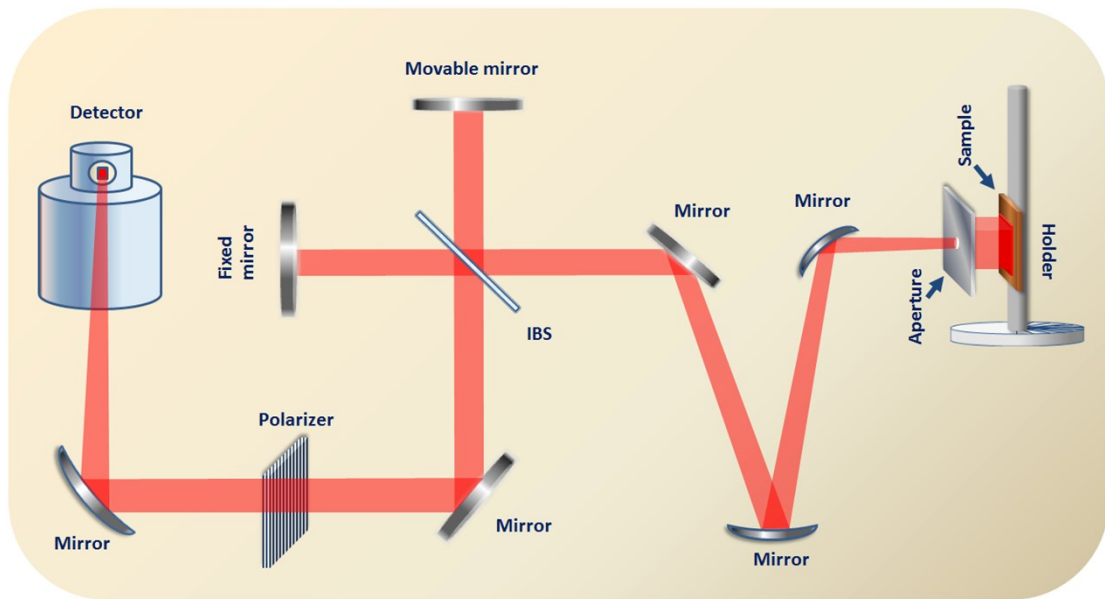


Figure S6 Schematic of the experimental setup for thermal emission measurements. IBS, infrared beam splitter. The thermal emitter sample was mounted on a homemade pillar holder which can be heated and rotated to measure the emission spectra in different angles.

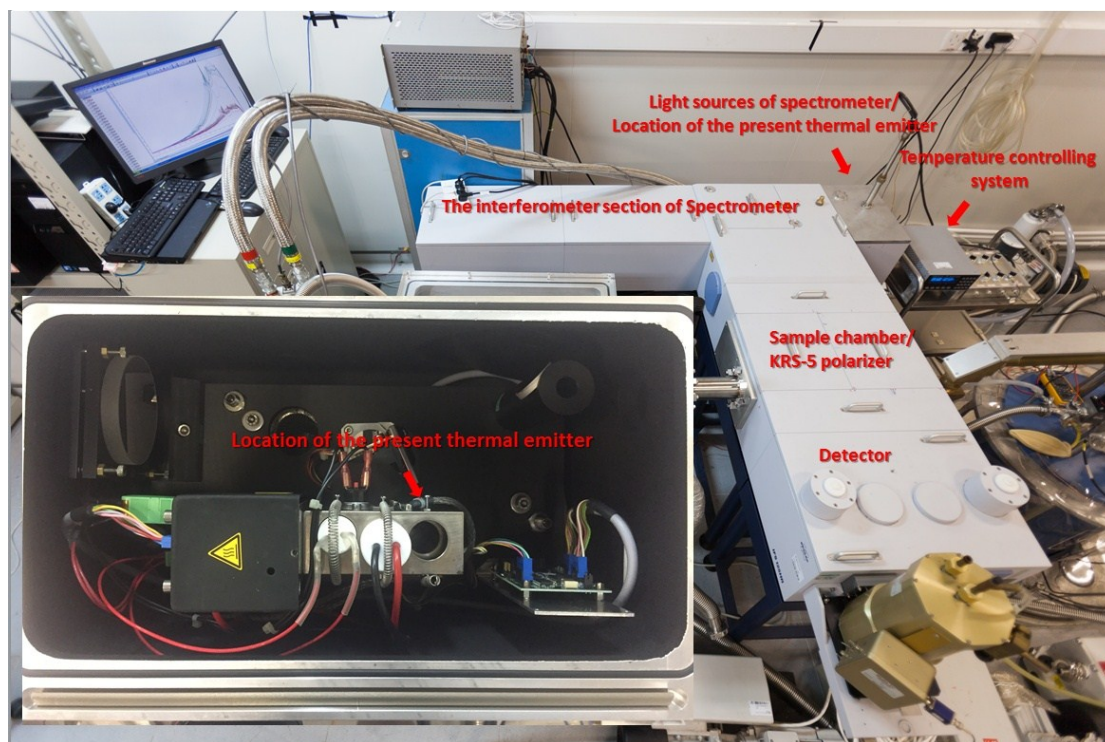


Figure S7 photograph of the experimental setup for optical characterizations. The angular polarized reflection and emission spectra of infrared narrow band emitter sample were conducted using a Fourier transform infrared spectrometer (Bruker IFS 125HR). For the emission measurement, the sample was mounted on a homemode holder, which can be heated and rotated to measure the emission spectra in different angles. For reflection/absorption characterization, due to the limitation of variable angle reflection accessory, the minimum allowable incident angle is 13° .

References

- [S1] H. H. Li, *J. Phys. Chem. Ref. Data*, 1980, **9**, 561.
- [S2] S. Ozaki and S. Adachi, *Jpn. J. Appl. Phys.*, 1993, **32**, 5008.
- [S3] G. Hawkins and R. Hunneman, *Infrared physics & technology*, 2004, **45**, 69.
- [S4] I. Celanovic, D. Perreault and J. Kassakian, *Phys. Rev. B*, 2005, **72**, 075127.
- [S5] J.-S. Bouillard, G. A. Wurtz, W. Dickson, D. O'Connor and A. V. Zayats, *Nano Lett.*, 2012, **12**, 1561.
- [S6] S. A. Uriri, T. Tashima, X. Zhang, M. Asano, M. Bechu, D. Ö. Güney, T. Yamamoto, Ş. K. Özdemir, M. Wegener and M. S. Tame, *Phys. Rev. A*, 2018, **97**, 053810.
- [S7] H. A. Haus, *Waves and Fields in Optoelectronics*, Prentice-Hall, Englewood Cliffs, NJ, **1984**.
- [S8] S. Fan, W. Suh and J. D. Joannopoulos, *J. Opt. Soc. Am. A*, 2003, **20**, 569.
- [S9] C. Qu, S. Ma, J. Hao, M. Qiu, X. Li, S. Xiao, Z. Miao, N. Dai, Q. He, S. Sun and L. Zhou, *Phys. Rev. Lett.*, 2015, **115**, 235503.
- [S10] P. Yeh, *Optical Wave in Layered Media*, Wiley, New York, **1988**.
- [S11] R. Ruppin, *Phys. Lett. A*, 2002, **299**, 309.
- [S12] X. Liu, T. Starr, A. F. Starr and W. J. Padilla, *Phys. Rev. Lett.*, 2010, **104**, 207403.
- [S13] X. Pan, H. Xu, Y. Gao, Y. Zhang, L. Sun, D. Li, Z. Wen, S. Li, W. Yu, Z. Huang, J. Wang, B. Zhang, Y. Sun, J. Sun, X. Meng, X. Chen, B. Dagens, J. Hao, Y. Shen, N. Dai and J. Chu, *Adv. Optical Mater.*, 2018, **6**, 1800337.